Vibration analysis on electromagnetic-resonance-ultrasound microscopy (ERUM) for determining localized elastic constants of solids

Jiayong Tian,[a] Hirotsugu Ogi, Toyokazu Tada, and Masahiko Hirao
Graduate School of Engineering Science, Osaka University, Machikaneyama 1-3, Toyonaka, Osaka 560-8531, Japan

(Received 13 June 2003; revised 14 November 2003; accepted 24 November 2003)

In this paper we present a new acoustic-resonance microscopy, Electromagnetic-Resonance-Ultrasound Microscopy (ERUM), to measure the localized elastic stiffness of a solid material. It visualizes the resonance-frequency shift of vibrating piezoelectric crystal (langasite, $La_3Ga_5SiO_{14}$) excited by an electric field from a solenoid coil. The acoustic coupling is made only at the tip of the crystal touching the specimen surface. Being based on the calibration for the specimen's effective stiffness, the local elasticity is determined from the resonance frequencies of the crystal with the Rayleigh–Ritz method. An approximate model for the specimen's effective stiffness predicts the shift of resonance frequencies, for which the conventional Hertz-contact model is improved. As an illustrating example, the mapping of Young's modulus of a duplex stainless steel is presented, which shows good agreement with the existing study. © *2004 Acoustical Society of America.* [DOI: 10.1121/1.1642618]

PACS numbers: 43.35.Yb, 43.58.Wc [RR] Pages: 630–636

I. INTRODUCTION

Many multiphase composites are emerging and the understanding of mechanical properties of the individual phases become more important. Especially, the local elastic constants are indispensable to predict the effective elastic stiffness, the strength, and the degree of degradation of the materials.

For measuring hardness and evaluating localized elastic constants, the indentation methods are widely used.[1] Recently, ultrasonic-atomic-force microscopy (UAFM) has been developed to measure the elastic properties in micro- and nanoscale regions of materials.[2–5] It excites a flexural vibration of a microcantilever by a piezoelectric transducer. The free end of the cantilever touches a specimen surface with an applied force. The technique is capable of mapping the elasticity difference within a spatial resolution of less than 100 nm. However, much research neglected considering influence of the mounted piezoelectric transducer on the vibration of the cantilever and that of the clamping condition at the fixed end. Particularly, the clamped end is not ideally the rigid end and this uncertain boundary condition prevents one from evaluating of the elastic stiffness.

Here, we present an alternative acoustic microscopy, *Electromagnetic-Resonance-Ultrasound Microscopy* (ERUM), to quantitatively evaluate the local stiffness of a material. It uses the resonance-frequency shift of a rectangular-parallelepiped piezoelectric probe, made of langasite ($La_3Ga_5SiO_{14}$), touching the specimen only through a tip. Langasite is a piezoelectric crystal and the vibrations are excited by applying dynamic electric fields using a surrounding solenoid coil. Thus, neither an electrode nor mechanical contact is required for the acoustic coupling. Such noncontact excitation and detection of ultrasonic vibrations eliminate the measurement errors associated with the contact coupling and the ambiguous boundary condition at the supports. Such a noncontacting excitation and the detection of vibration in a piezoelectric material was first reported by Choi and Yu,[6] then by Johnson *et al.*[7] Use of the noncontacting method for scanning the object surface to measure the elastic stiffness has not been reported. In this study, we measure the resonance-frequency shift of the probe and provide an elastic-constant distribution in a localized area.

Concerning the vibration analysis, we use Lagrangian-minimization approach with the Rayleigh–Ritz approximation[8–11] to calculate the resonance-frequency shift caused by a contact with the object solid. Because the conventional Hertz model does not apply to a dynamic contact,[12] we use an approximate approach for the dynamic-contact stiffening. Lastly, we apply this new acoustic microscopy to a duplex stainless steel consisting ferritic and austenitic phases. Determined Young's moduli of the two phases were consistent with the prediction previously reported.

II. ELECTROMAGNETIC-RESONANCE-ULTRASOUND MICROSCOPY

The measurement setup of ERUM is shown in Fig. 1. An oriented rectangular-parallelepiped langasite ($La_3Ga_5SiO_{14}$) crystal stands in a solenoid coil. It measures 10.012 mm ($=L_1$) by 10.043 mm ($=L_2$) by 14.405 mm ($=L_3$), respectively. Three principal crystallographic axes x_1, x_2, and x_3 are along the three sides L_1, L_2, and L_3, respectively. The mass density is 5731 kg/m^3. A spherical bearing of tungsten

[a]Electronic mail: J_tian@me.es.osaka-u.ac.jp

carbide is bonded at the center of the bottom surface (x_3 surface), through which the langasite crystal contacts the specimen fixed on an $X-Y$ stage. A weight provides a biasing force F_0 to the nodal points on the upper surface of the probe through three needles in order to minimize the mechanical contacts with the surroundings and then enhance the sensitivity of resonance-frequency shift.

Langasite is a trigonal-symmetry crystal, whose elastic constants C_{ij}, piezoelectric coefficients e_{ij}, and dielectric coefficients ϵ_{ij} are given as[11]

$$[C_{ij}]=\begin{bmatrix} 188.5 & 104.7 & 96.87 & 14.11 & 0 & 0 \\ & 188.5 & 96.87 & -14.11 & 0 & 0 \\ & & 263.11 & 0 & 0 & 0 \\ & & & 53.35 & 0 & 0 \\ & \text{sym.} & & & 53.35 & 14.11 \\ & & & & & 41.9 \end{bmatrix} \quad (\text{GPa}), \tag{1}$$

$$[e_{ij}]=\begin{bmatrix} -0.429 & 0.429 & 0 & 0.193 & 0 & 0 \\ 0 & 0 & 0 & 0 & -0.193 & 0.429 \\ 0 & 0 & 0 & 0 & 0 & 0 \end{bmatrix} \quad (\text{C/m}^2), \tag{2}$$

$$[\epsilon_{ij}]=\begin{bmatrix} 19.05 & 0 & 0 \\ & 19.05 & 0 \\ \text{sym.} & & 50.50 \end{bmatrix}\epsilon_0, \tag{3}$$

where ϵ_0 denotes the dielectric constant in vacuum. Thus, langasite's e_{11} and e_{14} are larger in magnitude than quartz's e_{11} and e_{14} by factors 2.5 and 4.4, respectively. Such favorable piezoelectricity allows us to excite the vibration effectively without any contacts with a dynamic electric field. Furthermore, the elastic constants of langasite show a weak dependence on temperature, of the order of $10^{-5}\,\text{K}^{-1}$,[13] which assures stable resonance frequencies.

We apply high-power rf bursts to the solenoid coil to cause the vibration of the probe by the converse piezoelectric effect. Then, the vibration of the probe is received by the same coil with the piezoelectric effect after the excitation.[11] The received signal is fed to a superheterodyne spectrometer to extract the signal amplitude of the same frequency component of the driving rf bursts.[14] A frequency scan provides a resonance spectrum as the one shown in Fig. 2, comprising a number of resonance peaks. The Lorentzian-fitting procedure to a peak yields the resonance frequency. We measure continuously the resonance frequency during moving the $X-Y$ stage to map the resonance-frequency shift.

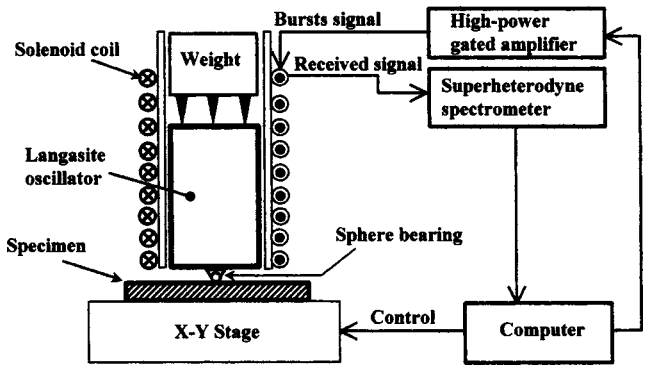

FIG. 1. Setup for ERUM.

III. VIBRATION ANALYSIS

We develop an approximated model to determine the localized Young's modulus of the specimen from the resonance-frequency shift of the probe. A simplified geometry of ERUM is shown in Fig. 3, where the tip–sample contact is equivalent to a support with springs having nonlinear spring constants k_{ij}. Here, we neglect the effect of contacts between the three needles and the crystal's upper surface because of three reasons: First, as shown later, the needles contact the nodal points of the out-of-plane displacement and affect little the out-of-plane vibrations. Second, the langasite crystal has mirror-finished surfaces, which allows almost frictionless contacts and then negligible influence on the in-plane displacement. Third, even if frictional and antinode contacts are considered, the contact areas at the needle tip are much smaller than that at the bearing–specimen contact and their influence again can be neglected, because the contact influence is enhanced with increasing the contact area, as seen in the Appendix.

The analysis contains two steps. First, we study the effect of the spring constants on the shift of the probe's resonance frequency. Second, we derive the relation between the localized Young's modulus of the specimen and the spring constants.

We adopt the Rayleigh–Ritz method for the first step. For a vibrating piezoelectric crystal with spring supports at the surface, Lagrangian Π can be expressed as[8–11]

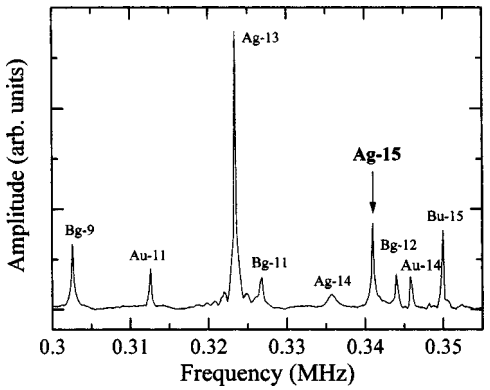

FIG. 2. Free-vibration resonance spectrum of a langasite probe measured by exiting the solenoid coil.

$$\prod = \frac{1}{2}\int\int\int_{\Omega} (S_{ij}C_{ijkl}S_{kl} + 2S_{ij}e_{ijk}\phi_{,k} - \phi_{,i}\epsilon_{ij}\phi_{,j} - \rho\omega^2 u_i u_i)dV + \frac{1}{2}\int\int_{\Gamma} \tilde{k}_{ij}u_j u_i\, dS, \tag{4}$$

where S_{ij}, ρ, u_i, and ϕ_i are the strain tensor, mass density, displacement, and electric potential, respectively. $\tilde{k}_{ij}$ are the surface distributed spring constants with dimension N/m^3. Ω and Γ denote the volume and surface of the piezoelectric crystal, respectively. We assume that $\tilde{k}_{ij}=0$ for $i\neq j$. Because no analytical solutions for u_i and ϕ exist, we approximately express the displacement vector $\mathbf{U}=[u_1,u_2,u_3]^T$ and the electric potential ϕ in the linear combination of orthogonal basis functions $\mathbf{Y}$,

$$\mathbf{U}=\mathbf{Ya}, \tag{5}$$

$$\phi=\mathbf{Yb}, \tag{6}$$

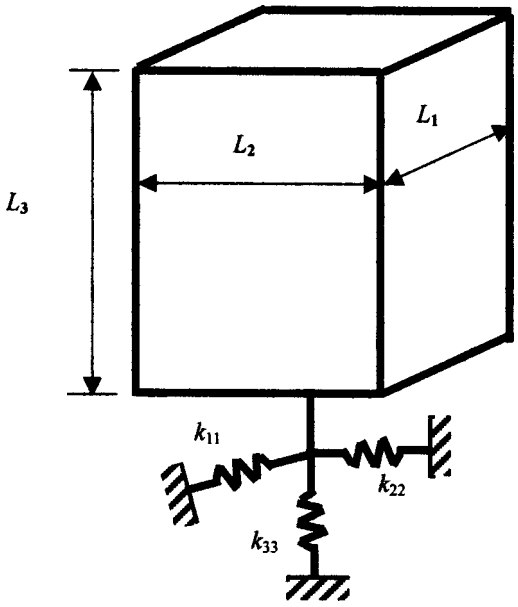

FIG. 3. Contact model of the tip.

where **a** and **b** are unknown coefficient vectors. We select Legendre polynomials P_k as the orthogonal base, which is given as

$$Y^{(p)}(x_1,x_2,x_3) = \frac{1}{\sqrt{L_1L_2L_3}}\sqrt{\frac{2k+1}{2}}\sqrt{\frac{2m+1}{2}} \times \sqrt{\frac{2n+1}{2}}P_k\left(\frac{x_1}{L_1}\right)P_m\left(\frac{x_2}{L_2}\right)P_n\left(\frac{x_3}{L_3}\right). \tag{7}$$

Note that the base functions **Y** show the orthogonality relationship:

$$\int\int\int_{\Omega} Y^{(p)}Y^{(p')}d\Omega = \delta_{kk'}\delta_{mm'}\delta_{nn'}, \tag{8}$$

where δ_{ij} denotes Kronecker's delta function. The substitution of Eqs. (5) and (6) into Eq. (4) yields

$$\prod = \frac{1}{2}\mathbf{a}^T\mathbf{K}\mathbf{a} + \mathbf{b}^T\mathbf{K}_1\mathbf{a} - \frac{1}{2}\mathbf{b}^T\mathbf{K}_2\mathbf{b} - \frac{1}{2}\omega^2\mathbf{a}^T\mathbf{M}\mathbf{a} + \frac{1}{2}\mathbf{a}^T\mathbf{K}_3\mathbf{a}, \tag{9}$$

where $K_{pp'}=\int\int\int_{\Omega} S_{ij}(Y^{(p)})C_{ijkl}S_{kl}(Y^{(p')})d\Omega$, $K_{1pp'}=\int\int\int_{\Omega} Y^{(p)}_{,i}e_{ikl}S_{kl}(Y^{(p')})d\Omega$,

$$K_{2pp'}=\int\int\int_{\Omega} Y^{(p)}_{,i}\epsilon_{ij}Y^{(p')}_{,j}\,d\Omega,$$

$$K_{3pp'}=\int\int\int_{\Gamma} Y^{(p)}_{i}\tilde{k}_{ij}Y^{(p')}_{j}dS, \quad \text{and } M_{ij}=\rho\delta_{ij}.$$

Applying the variational principle that implies the minimization of Eq. (9) with respect to **a** and **b**, we obtain

$$\mathbf{K}\mathbf{a}+\mathbf{K}_1^T\mathbf{b}+\mathbf{K}_3\mathbf{a}-\omega^2\mathbf{M}\mathbf{a}=0, \tag{10}$$

$$\mathbf{K}_2\mathbf{b}-\mathbf{K}_1\mathbf{a}=0. \tag{11}$$

Substituting Eq. (11) into Eq. (10), we obtain the characteristic equation for resonance frequencies,

$$|\mathbf{K}+\mathbf{K}_1^T\mathbf{K}_2^{-1}\mathbf{K}_1+\mathbf{K}_3-\omega^2\mathbf{M}|=0, \tag{12}$$

as well as the corresponding eigenvectors.

Langasite belongs to the trigonal system with point group 32. Free vibrations of an oriented rectangular parallelepiped of such a material fall into four groups labeled Ag, Au, Bg, and Bu,[11] whose displacement symmetry is given in Table I.

For the second step, we consider a simplification for the tip–sample contact. Figure 4 shows the detailed geometry of the tip. The tip consists of a steel base and the spherical tungsten–carbide bearing with 0.35 mm radius. The bearing can rotate, contacting the specimen. The steel base is bonded to the center of the crystal's bottom surface with the contact area of 0.6 mm radius.

The previous UFAM studies used the simple Hertz-contact model as summarized in the Appendix to calculate

TABLE I. Vibration modes of piezoelectric crystal with trigonal symmetry of elastic constants. O and E represent odd and even functions, respectively.

	k	$m+n$		k	$m+n$		k	$m+n$		k	$m+n$
u_1	O	E	u_1	E	E	u_1	E	O	u_1	O	O
u_2	E	O	u_2	O	O	u_2	O	E	u_2	E	E
u_3	E	O	u_3	O	O	u_3	O	E	u_3	E	E
ϕ	O	E	ϕ	E	E	ϕ	E	O	ϕ	O	O
	Ag			Au			Bg			Bu	

the effective contact stiffness. However, this model fails to explain the resonance-frequency shift as shown later in Fig. 7 and as discussed elsewhere.[12] We then seek a relationship between the specimen Young's modulus and resonance-frequency shift with an empirical rule as follows.

According to the Hertzian-contact theory,[15] the effective spring stiffnesses are expressed by a power law of the equivalent Young's modulus E^* or shear modulus G^*,

$$k_{33}=AE^{*\delta_1}, \tag{13}$$

$$k_{11}=k_{22}=BE^{*\delta_2}G^{*\delta_3}, \tag{14}$$

where $1/E^*=(1-\nu_1^2)/E_1+(1-\nu_2^2)/E_2$ and $1/G^*=(2-\nu_1)/G_1+(2-\nu_2)/G_2$; E, G, and ν are Young's modulus, shear modulus, and Poisson's ratio. The subscripts 1 and 2 indicate the bearing and the specimen, respectively. δ_1, δ_2, and δ_3 denote power factors. Coefficients A and B depend on the applied biasing force and shape of contacting elements. The analytical solution for contact problem is limited to a few simple cases: For example, $\delta_1=2/3$, $A=\sqrt[3]{6RF_0}$, and $\delta_2=-1/3$, $\delta_3=1$, $B=\sqrt[3]{128RF_0}$ for a normal contact of two elastic spheres without slip (a frictional contact). (When the specimen surface is well flat (mirror finish), the tangential spring constants can be negligible.) Thus, assuming that the normal spring stiffness and tangential spring stiffness show similar exponential dependences on E^* and G^* as in Eqs. (13) and (14), we determine the unknown coefficients and power factors through calibration measurements.

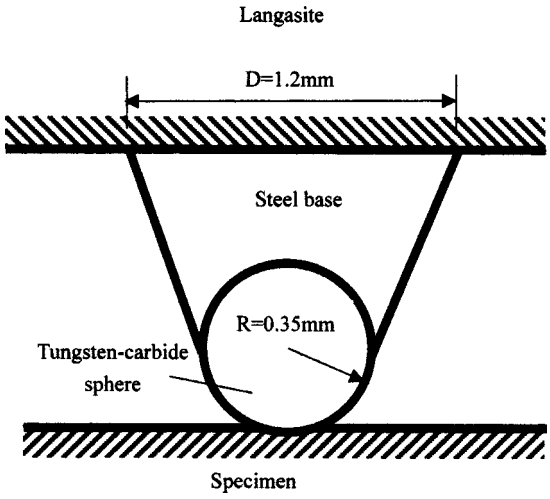

FIG. 4. Close-up of the tip for ERUM.

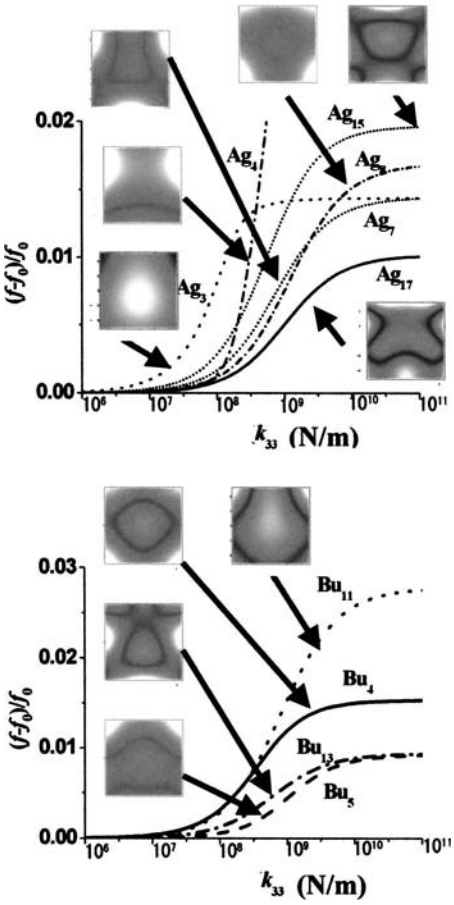

FIG. 5. Influence of the normal stiffness k_{33} on resonance frequencies for Ag and Bu groups.

IV. RESULT AND DISCUSSION

To study the effect of the normal spring constant k_{33} independently, we calculated the dependence of resonance frequencies of Ag and Bu modes on k_{33} using Eq. (12) with $k_{11}=k_{22}=0$. The result is shown in Fig. 5. Figure 5 also shows corresponding distributions of normal displacement u_3 at the probe's upper surface, which are calculated from eigenvectors associated with Eq. (12) for free vibrations. Because Au and Bg modes show a nodal line for u_3 passing the center of the bottom surface, where the tip is attached, the normal spring constant k_{33} has no influence on these modes. Shifts of resonance frequencies of Ag and Bu modes increase with increasing k_{33}. They increase with high sensitivity for $k_{33}=10^7-10^9$ N/m and show saturation with larger k_{33} values. When k_{33} is smaller than 10^8 N/m, Ag-3, Ag-15, Bu-4, and Bu-11 modes show larger sensitivity to k_{33} than others. Figure 5 predicts the largest sensitivity of Ag-3 mode to the specimen modulus (or k_{33}), but we failed to observe this mode because of the limited frequency range of the measuring instrument we used. Also, we failed to detect Bu modes with the solenoid coil we used. Hence, we use the Ag-15 mode as a most suitable mode for the present ERUM measurements because (i) this mode has relatively high sensitivity to the material stiffness (Fig. 5); (ii) it demonstrates a good spectral lineshape (see Fig. 2) and no mode overlapping occurs at its frequency; and (iii) the resonance frequency shows a small normalized temperature derivative of

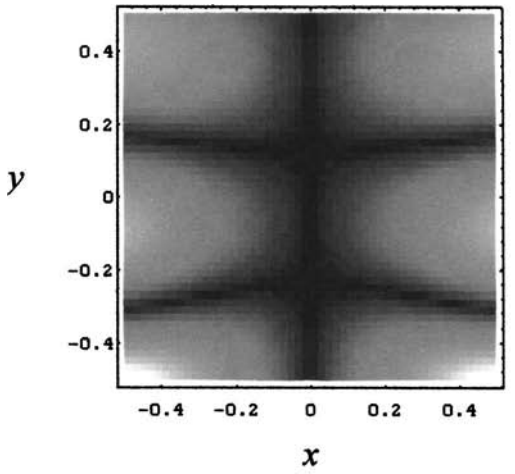

(a) u_1

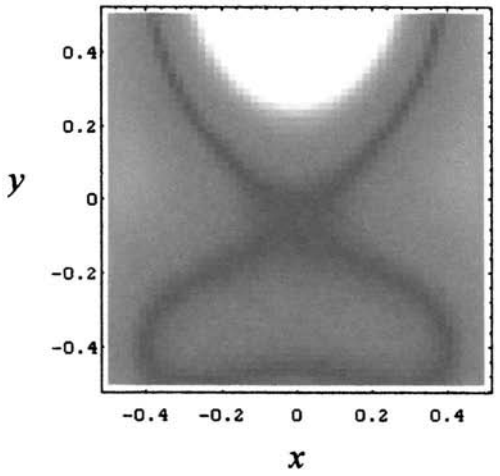

(b) u_2

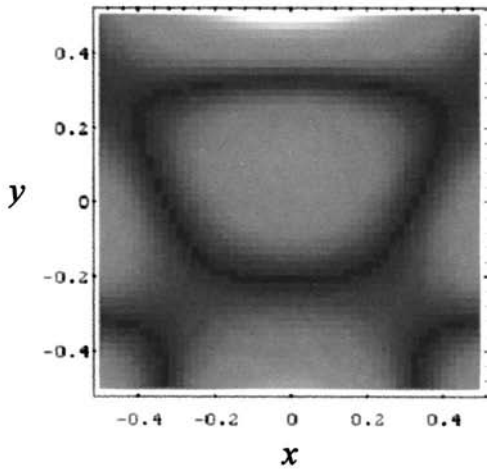

(c) u_3

FIG. 6. The modal profile of Ag-15 resonance at the upper surface of a langasite probe.

$2.3\times10^{-5}\,\mathrm{K}^{-1}$ for the 25 °C–35 °C range, which is much smaller than that of common metals; and (iv) this mode shows nodal points for the in-plane displacements u_1 and u_2 at the center of the bottom surface, as shown in Fig. 6, which allows us to neglect the tangential spring constants k_{11} and k_{22} to make the problem much simpler. [Indeed, we calculated the effect $k_{11}(=k_{22})$ on the Ag-15 mode and verified its negligible contribution.] Thus, only the normal spring constant k_{33} affects the Ag-15 resonance frequency with unknown coefficients δ_1 and A.

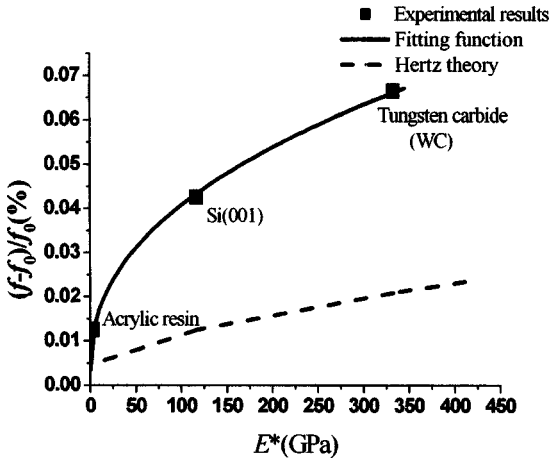

FIG. 7. A comparison between the fitting curve and Hertz theory (f_0: free vibration frequency of Ag-15).

We measured the resonance frequency of the Ag-15 mode by making the probe contact acrylic resin, (001) surface of monocrystal silicon, and polycrystalline tungsten carbide with a static force of $F_0=0.4151\,\mathrm{N}$. We then inversely determined the unknown coefficients as $A=168.12\,\mathrm{N}^{0.66}\,\mathrm{m}^{0.22}$ and $\delta_1=0.44$ by a least-square fitting with Eq. (13). Figure 7 shows the comparison between the fitting function and the measurements along with a prediction by the classical Hertz theory. The Hertz model gives a similar dependence of the frequency shift on E^*, but the magnitude is only one-fourth of that of observations, indicating that the model is inapplicable to a quantitative evaluation of specimen's modulus.

To demonstrate the applicability of our method, we obtained the elastic-constant image of a duplex stainless steel (JIS-SCS14A).[16] The material consists of 25.8% volume fraction of α (ferrite) phase and 74.2% volume fraction γ (austenite) phase. Figure 8 shows the microstructure. The γ-phase particles are precipitated in the α-phase matrix. Figure 9(a) is the ERUM image obtained by scanning the specimen surface at every 5 μm. A line trace of resonance-frequency shift is given in Fig. 9(b). We observe the resonance-frequency shift of the order of 10^{-4}. A larger shift occurs for the γ phase. Using a plausible value of 0.25 for

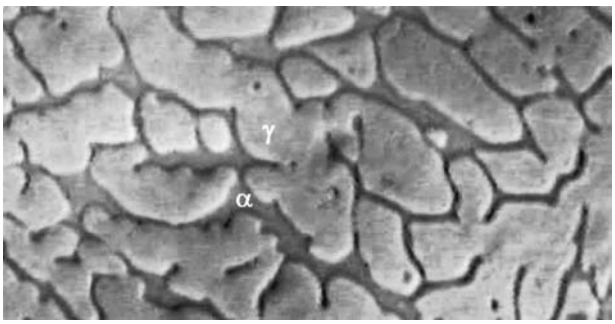

FIG. 8. Optical microstructure of a duplex stainless steel (JIS-SCS14A).

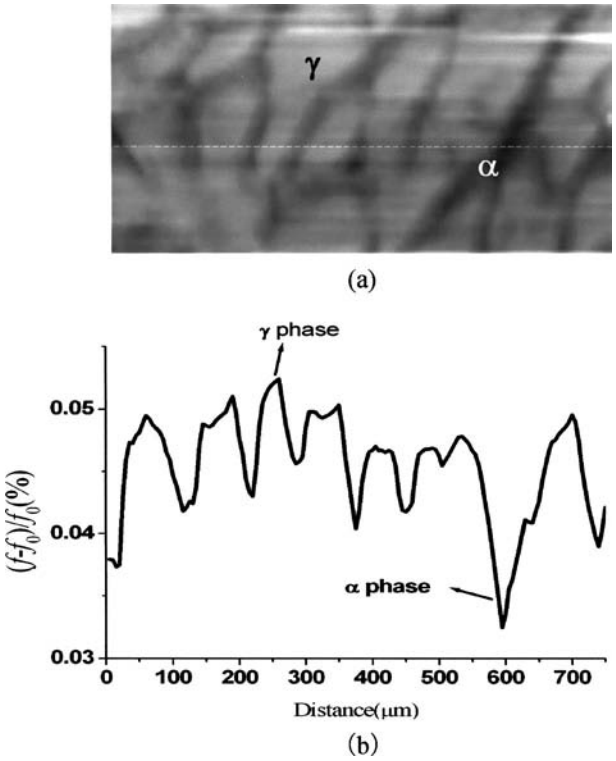

FIG. 9. (a) ERUM image of the surface of duplex stainless steel and (b) the line trace of the resonance-frequency shift, as indicated in (a).

Poisson's ratio, the fitting curve in Fig. 7 gives the grain-average Young's moduli of two phases as $E_\gamma = 219$ GPa and $E_\alpha = 128$ GPa. [Note that the specimen's Poisson ratio has an insignificant influence on the effective Young's modulus E^* because $(1-\nu^2)$ affects the modulus.] Young's modulus of γ phase agrees with that of austenitic stainless steels ($E_\gamma = 215$ GPa in Ref. 15). Young's modulus E_α is, however, considerably small compared with that of ferritic steels ($E_\alpha = 212$ GPa in Ref. 15). This is possible, considering the fact that large concentration of Cr in the α phase elongates the atomic distance. The lattice parameter of the α phase measured for the same material is 2.93 Å,[16] which is fairly larger than that of standard ferritic steels (2.87 Å). Thus, the elastic constants can reduce because of the lattice's anharmonic effect. Tane *et al.*[16] estimated the α-phase Young's modulus of the same material using a micromechanics calculation, and they gave 158 GPa, which is actually much smaller than that of standard ferritic steel by 34% and closer to our value.

V. CONCLUSION

Being based on the vibration of langasite crystal measured by the noncontacting electromagnetic-acoustic-resonance technique, ERUM shows high potential of measuring the local elastic constant of solids. The Ag-15-mode is selected for the operating mode of ERUM because of the high sensitivity to specimen modulus and the stability to temperature change. The approximate contact model is proposed by improving the basis of the conventional Hertz model. We find that the proposed approach is suitable for a quantitative evaluation of the localized modulus. The technique was applied to measure the Young-modulus distribution on a duplex stainless steel. The results show favorable agreement with the previous reports.

ACKNOWLEDGMENT

The first author (J. T.) acknowledges the support provided by Japan Society for the Promotion of Science (JSPS).

APPENDIX: HERTZ MODEL OF TIP–SAMPLE CONTACT

According to Hertz theory,[15] the contact radius a and indentation depth d of the sphere under a normal force F can be written as

$$a = \sqrt[3]{\frac{3FR}{4E^*}} \quad \text{and} \quad d = \sqrt[3]{\frac{9F^2}{16E^{*2}R}},$$

where R is the radius of the tip. The initial indentation depth d_0 can be expressed as

$$d_0 = \sqrt[3]{\frac{9F_0^2}{16E^{*2}R}}.$$

The vertical displacement at a contact point for a vibrating probe is then written as

$$u_z|_B = d - d_0 = \sqrt[3]{\frac{3F_0^2}{16E^*R}} - \sqrt[3]{\frac{3F_0^2}{16E^*R}}.$$

Because the vibration amplitudes of ERUM are of very small magnitude and F_0 is much greater than $|F-F_0|$, the vertical displacement at a contact point can be approximated to be

$$u_z|_B \approx \frac{(F-F_0)}{k_{33}},$$

by a Taylor expansion. Here $k_{33} = \sqrt[3]{6E^{*2}RF_0}$ is the effective normal-contact spring stiffness of the tip–sample contact.

If the tangential force Q_x and Q_y act and induce the elastic deformation without slip, the relative displacement between the sample and the tip can be expressed as

$$u_x = \frac{Q_x}{k_{11}} \quad \text{and} \quad u_y = \frac{Q_y}{k_{22}},$$

where $k_{11} = k_{22} = 8aG^*$ is the effective tangential-contact spring stiffness of the tip–sample contact.

[1] E. M. Uygur, "Nondestructive dynamic testing," *Research Techniques in Nondestructive Testing*, edited by R. S. Sharpe (Academic, New York, 1980), Vol. 4, pp. 205–244.

[2] K. Yamanaka and S. Nakano, "Quantitative elasticity evaluation by contact resonance in an atomic force microscopy," Appl. Phys. A: Mater. Sci. Process. **66**, S313–S317 (1998).

[3] K. Yamanaka, A. Noguchi, T. Tsuji, T. Koike, and T. Goto, "Quantitative material characterization by ultrasonic AFM," Surf. Interface Anal. **27**, 600–606 (1999).

[4] U. Rabe, J. Turner, and W. Arnold, "Analysis of the high-frequency response of atomic force microscopy cantilevers," Appl. Phys. A: Mater. Sci. Process. **66**, S277–S282 (1998).

[5] E. Kester, U. Rabe, L. Presmanes, Ph. Taihades, and W. Arnold, "Measurement of mechanical properties of nanoscaled ferrites using atomic force microscopy at ultrasonic frequencies," Nanostruct. Mater. **12**, 779–782 (1999).

[6] K. Choi and I. Yu, "Inductive detection of piezoelectric resonance by

using a pulse NMR/NQR spectrometer,'' Rev. Sci. Instrum. **60**, 3249–3252 (1989).
[7] W. Johnson, S. Kim, and D. Lauria, ''Anelastic loss in langatate,'' in *Proceedings of the IEEE/EIA International Frequency Control Symposium and Exhibition*, 2000, pp. 186–190.
[8] H. Ogi, P. Heyliger, H. Ledbetter, and S. Kim, ''Mode-selective resonance ultrasound spectroscopy of a layered parallelepiped,'' J. Acoust. Soc. Am. **108**, 2829–2834 (2000).
[9] I. Ohno, ''Rectangular parallelepiped resonance method for piezoelectric crystals and elastic constants of alpha-quartz,'' Phys. Chem. Miner. **17**, 371–378 (1990).
[10] A. Migliori, J. Sarrao, W. Visscher, T. Bell, M. Lei, Z. Fisk, and R. Leisure, ''Resonant ultrasonic spectroscopy techniques for measurement of the elastic moduli of solids,'' Physica B **183**, 1–24 (1993).
[11] H. Ogi, N. Nakamura, K. Sato, M. Hirao, and S. Uda, ''Elastic, anelastic, and piezoelectric coefficient of langasite: resonance ultrasound spectroscopy with laser-Doppler interferometry,'' IEEE Trans. Ultrason. Ferroelectr. Freq. Control **50**, 553–560 (2003).
[12] J. Y. Tian, H. Ogi, and M. Hirao, ''Vibration analysis for an elastic-sphere oscillator contacting semi-infinite viscoelastic solids in resonance ultrasound microscopy,'' J. Appl. Phys., to be published.
[13] A. Bungo, C. Jian, K. Yamaguchi, Y. Sawada, S. Uda, and Y. Pisarevsky, ''Analysis of surface acoustic wave properties of the rotated Y-cut langasite substrate,'' Jpn. J. Appl. Phys. **38**, 3239–3243 (1999).
[14] M. Hirao, H. Ogi, and H. Fukuoka, ''Resonance EMAT system for acoustoelastic stress evaluation in sheet metals,'' Rev. Sci. Instrum. **64**, 3198–3205 (1993).
[15] K. L. Johnson, *Contact Mechanics* (Cambridge University Press, Cambridge, 1985).
[16] M. Tane, T. Ichitsubo, H. Ogi, and M. Hirao, ''Elastic property of aged duplex stainless steel,'' Scr. Mater. **48**, 229–234 (2003).